International Journal of Mass Spectrometry 281 (2009) 140–149

Contents lists available at ScienceDirect

International Journal of Mass Spectrometry

journal homepage: www.elsevier.com/locate/ijms

A laser desorption–electron impact ionization ion trap mass spectrometer for real-time analysis of single atmospheric particles

E.A. Simpson, P. Campuzano-Jost*, S.J. Hanna, D.B. Robb, J.H. Hepburn, M.W. Blades, A.K. Bertram

Department of Chemistry, University of British Columbia, Vancouver, BC V6T 1Z1, Canada

ARTICLE INFO

Article history:
Received 31 October 2008
Received in revised form 20 January 2009
Accepted 22 January 2009
Available online 31 January 2009

Keywords:
Aerosol mass spectrometry
Single particle analysis
Particle laser vaporization
Electron impact ionization

ABSTRACT

A novel aerosol ion trap mass spectrometer combining pulsed IR laser desorption with electron impact (EI) ionization for single particle studies is described. The strengths of this instrument include a two-step desorption and ionization process to minimize matrix effects; electron impact ionization, a universal and well-characterized ionization technique; vaporization and ionization inside the ion trap to improve sensitivity; and an ion trap mass spectrometer for MS^n experiments. The instrument has been used for mass spectral identification of laboratory generated pure aerosols in the 600 nm–1.1 μm geometric diameter range of a variety of aromatic and aliphatic compounds, as well as for tandem mass spectrometry studies (up to MS^3) of single caffeine particles. We investigate the effect of various operational parameters on the mass spectrum and fragmentation patterns. The single particle detection limit of the instrument was found to be a 325 nm geometric diameter particle (8.7×10^7 molecules or 22 fg) for 2,4-dihydroxybenzoic acid. Lower single particle detection limits are predicted to be attainable by modifying the EI pulse. The use of laser desorption-electron impact (LD-EI) in an ion trap is a promising technique for determining the size and chemical composition of single aerosol particles in real time.

1. Introduction

Aerosols are an important topic of research given their ubiquitous presence in the atmosphere and their significant role in both climate and human health [1]. Atmospheric aerosols contain numerous species including sulfates, nitrates, and organics. A very significant mass fraction (20–90%) of the submicron aerosol component is composed of, or contains, organic molecules [2]. The challenges in their characterization lie in their enormous variety and complexity, as well as their fragility under analysis [3].

Aerosol mass spectrometry has emerged as an extremely powerful technique for investigating organic and inorganic particles in both the field and the laboratory. Although the majority of aerosol mass spectrometers employ either a linear quadrupole or TOF-MS [4–14], ion trap mass spectrometers have been successfully used for single particle analysis for more than a decade [15–23]. The ion trap offers a multitude of desirable properties: versatility, compact size, high duty cycle, high sensitivity, full spectrum collection for single particles, large accessible mass range, and tandem mass spectrometry capabilities for further speciation. Some of the different versions of aerosol mass spectrometers that incorporate an ion trap are discussed below.

Ion trap instruments can be divided into two categories based on the process used for particle ionization: (1) a single step desorption/ionization and (2) a two-step desorption and ionization of the particle. Single step laser desorption ionization (LDI) was mostly applied in the earlier designs of aerosol ion trap spectrometers [17,20]. It works extremely well for detecting multiple components of single particles, however, it suffers from poor signal reproducibility, matrix effects, and a chemical bias towards certain species [24,25].

Two-step desorption ionization processes include both laser based and thermal based methods for the desorption step. Two-step laser desorption and ionization (L2MS) provides flexibility for the optimization of each process, requires lower laser intensities, and gives less fragmentation for organic compounds compared to the single step laser desorption ionization [19]. Conversely, the ionization process is not as universal as LDI or electron impact (EI) in most cases and presents certain challenges with respect to the alignment, focusing, and timing of two lasers [26].

Two-step thermal desorption and ionization methods provide an experimentally simple and relatively universal means of vaporization, while allowing flexibility in the ionization step. Types of ionization used with thermal desorption have included electron impact ionization [27], chemical ionization [28], and atmospheric sampling glow discharge ionization [29]. Thermal vaporization with EI provides quantitative capabilities and a large library of standard mass spectra for comparison. It has been successfully used with quadrupole and time of flight mass spectrometers for

* Corresponding author.
E-mail address: pcampuzano@chem.ubc.ca (P. Campuzano-Jost).

1387-3806/$ – see front matter © 2009 Elsevier B.V. All rights reserved.
doi:10.1016/j.ijms.2009.01.013

quantitative aerosol measurements of total carbon compounds and substance class grouping [7,8], however, the implementation of thermal vaporization with EI is difficult within an ion trap due to the geometric constraints and possible trapping field disturbances. To overcome these barriers, ions are generally created outside of the trap in existing ion trap mass spectrometers for aerosol analysis [21,27], for which Kürten et al. [21] estimate a 1–5% trapping efficiency, in line with similar efficiencies measured for electrospray ionization outside an ion trap [30].

Here we develop a new type of ion trap mass spectrometer for single particle analysis, which incorporates a pulsed CO_2 laser for in-trap desorption and 70 eV electron impact ionization. The decoupled desorption and ionization steps should ensure signal reproducibility, minimize charge-transfer matrix effects and extensive fragmentation of neutrals, and help preserve quantitative mass capabilities [31,32]. While Kürten et al. [21] and Harris et al. [27] both employ EI with an ion trap, our design is notably different in that vaporization is achieved with a CO_2 laser rather than a heater cartridge. This enables single particle analysis and since the vaporization and ionization steps occur inside the trap should result in improved sensitivity and facilitate single particle measurements.

A mid-IR CO_2 laser for desorption [14,32–35] has several advantages over other laser vaporization methods: a low photon energy that allows for high fluencies before ionization takes place [36], minimization of the self-focusing effect for submicron particles, which reduces both inhomogeneous heating and preferential surface desorption [37], and a fairly long pulse width that reduces the possibility of particle shattering [38–40]. Additionally, many organics exhibit some absorption in the accessible wavelength range of a tunable CO_2 laser (9.2–10.8 μm).

In comparison to a cartridge heater, laser desorption results in superior gas-phase background discrimination and does not suffer effects from particle bounce [41]. On the other hand, using a pulsed laser requires a single particle triggering scheme that is complex and often leads to lower particle hit rates than particle heater impaction (especially for smaller particles). The LD-EI-ion trap mass spectrometer avoids matrix effects by separating the desorption and ionization steps, similar to L2MS techniques, but without the added cost and complexity of a second laser. EI provides useful information with linear and reproducible ionization of gas-phase molecules, multi-species applicability, quantitative capabilities, and a large library of standard spectra for comparison [7,42]. In addition, with an ion trap mass analyzer, tandem mass spectrometry can be performed for structural identification of more robust species [20,21,27]. LD-EI has been employed previously for bulk phase studies [43–49], but to the authors' knowledge no single particle studies have been conducted with this technique.

In this paper our new single particle mass spectrometer, which combines pulsed IR desorption with EI ionization, is described in detail. A preliminary characterization of the LD-EI technique follows. The instrument provides sizing and compositional information without matrix effects. The mass spectra obtained for aerosols of three different compounds (liquid and solid phase) are comparable to the reference NIST mass spectra. MS^3 studies were successfully performed. We also investigated the influence of vaporization energy and electron gate width on total ion signal and the effects of ionization delay on the degree of fragmentation. Results from 2,4-dihydroxybenzoic acid particles gave a detection limit of 325 nm (22 fg).

2. Experimental

A schematic of the instrument is shown in Fig. 1. As in most real-time aerosol mass spectrometers [17,41,50–52], our single particle ion trap mass spectrometer (SPIT-MS) consists of three distinct regions, briefly described by Hanna et al. [53]:

- A particle concentration and focusing region where an aerosol lens is used to collimate particles between 0.1 and 1 μm diameter into a tight particle beam [54,55]. This also serves as an interface between atmospheric pressure and the vacuum of the system.
- A particle sizing and trigger source region based in part on the work by Su et al. Particle velocity is determined by the timing of two scattering events [56] produced as the collimated aerosol beam transverses two focused continuous wave (532 nm) laser beams. Aerodynamic particle sizes are extrapolated from the terminal velocities imparted during the vacuum expansion. Custom, real-time data acquisition software records the timing and scattering signals and generates the appropriate triggers for the mass analysis region.
- A mass analysis region comprised of an IR laser for particle desorption, an electron gun for ionization, and the ion trap mass spectrometer.

2.1. Particle focusing region

An aerosol lens consists of a series of apertures of decreasing size where each successive aperture focuses a range of particles sizes with a Stokes number around 1 while particles already traveling along the centerline remain undisturbed. Our design uses the original set of aperture sizes reported by Liu et al. [54] (5, 4.5, 4, 3.5, 3 mm thin lenses followed by a 6 mm diameter capillary with a 3 mm thin lens which forms the nozzle) positioned at 5 cm intervals. Particles are sampled from atmosphere through a 100 μm critical orifice followed by a 25 cm long equilibration region (13 mm ID) and then enter the aerosol lens. This results in a sampling flow of 87 cm^3/min and a pressure of 1.6 Torr at the entry of the aerosol lens. This set of lenses has been shown to provide good focusing and >90% transmission for particle sizes roughly between 0.1 and 1 μm [55,57,58]. As the particles exit the nozzle of the lens, they undergo a supersonic vacuum expansion and achieve terminal velocities between 50 and 400 m/s thereby creating a tight particle beam [58,59]. The aerosols exit the lens into a differential pumping chamber pumped by a turbomolecular pump (V301, Varian Inc.) that attains a pressure of 1.4×10^{-2} Torr when the system is sampling aerosols. A high performance *X*–*Y* stage (Thermionics) with 1 μm resolution was used for aligning the aerosol lens with the mass analysis region.

2.2. Particle sizing region

Particles pass through the differential pumping chamber and enter the sizing region through a 5 mm skimmer. The sizing region, which is operated at approximately 7×10^{-5} Torr, is pumped by a second turbo pump (Varian 300HT). Within the sizing region particle velocities are determined by measuring the delay between two aerosol scattering events 6 cm apart. Two different configurations were used for this purpose.

In the first sizing configuration of the instrument (referred to as one laser setup in the following) a single scattering laser (100 mW 532 nm cw DPSS YAG; Crystalaser Ltd.) was split into 2 beams and focused via a telescope system to ~80 μm spot sizes for sizing detection. In this setup, small, reproducible adjustments in the vertical position of the laser beams were necessary for optimal sizing efficiencies near the extremes of the calibration aerosol (PSL) size range used (e.g., <300 nm and >700 nm) to compensate for the gravitational settling of larger particles. An 800 nm PSL particle drops about 30 μm at the second timing point relative to a 400 nm particle.

In the second setup (two laser setup), two single mode 100 mW 532 nm cw Nd:YAGs (Spectra-Physics Excelsior) are focused by sin-

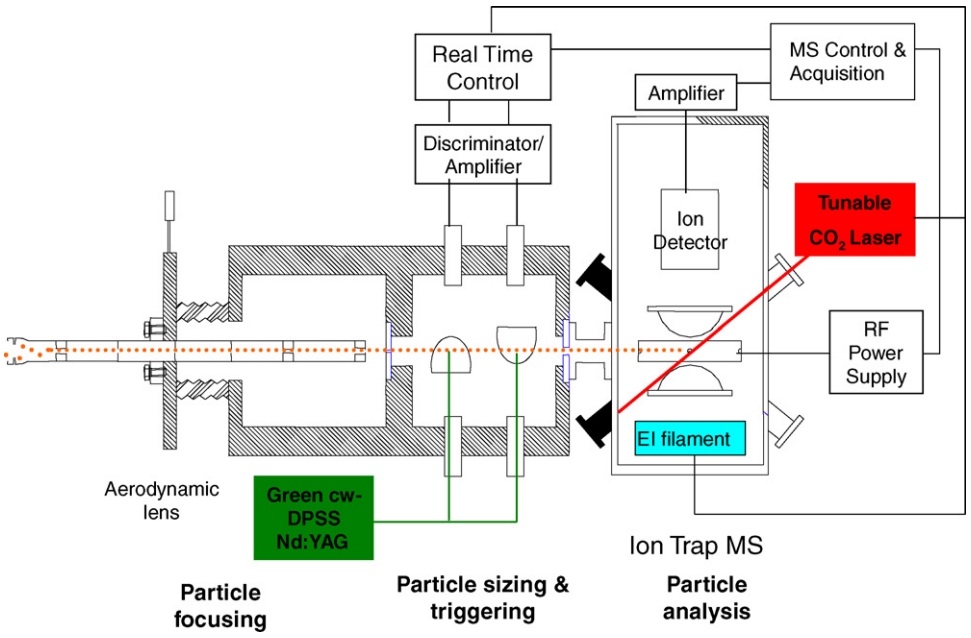

Fig. 1. Instrument setup of SPIT-MS for LD-EI.

gle lenses to ~280 μm laser spots. In this setup, which is also the current setup, the use of 2 lasers provides higher power and independent alignment of each scattering incident. The laser spot size of 280 μm is a compromise that allows for high detection efficiencies of spherical particles 300 nm and above without any adjustment in the vertical position of the laser beam to compensate for particle settling. The lasers were aligned to give optimal detection for the 600–700 nm vertical deflection point. The two laser setup was used for all mass spectrometric measurements reported in this paper.

The scattered light is collected by two custom elliptical mirrors (f = 101 mm, Optiform Ltd.) with four 2 mm apertures drilled at 90 degrees to allow passage of the particle and the laser beam [9,56]. The mirrors are mounted at opposing 45° angles relative to the instrument centerline on custom machined y–z stages and the collected light is directed onto two miniature photomultipliers (PMT 9001 V, Electron Tubes Ltd.) located close to the focus of the mirrors. The scattering signals are amplified by a shaping amplifier and discriminated with a single channel pulse analyzer (Ortec 590 A), generating TTL pulses with a maximal 50 ns jitter relative to the maxima of the scattering pulses.

The SPIT-MS uses an FPGA board (PCI-7831R, National Instruments) to record the particle velocities, generate the laser triggers and record other relevant particle information such as scattering signal size for the analyzed particle. It also generates the clock for the MS acquisition software and can phase lock all triggers and waveforms in the system. By using a real-time software solution instead of hardware counters, it is possible to acquire size information independently from the actual triggering, so that particle size distributions of sampled aerosols (as opposed to analyzed aerosols) can be accessed at any given time. With typical settings (1.25 μm aerodynamic diameter upper cutoff), about 1000 particles/s (i.e., ~700 particles/cm^3) can be accurately sized.

2.3. Particle mass analysis region

2.3.1. Desorption and ionization

After exiting the second scattering mirror, the particles enter the vacuum chamber housing the mass spectrometer, pumped by a third turbo pump (Varian V300HT). For design and testing convenience, the sizing and detection module are located in two separate chambers. Aerosols enter the 3D ion trap (approximately 41 cm from the exit of the aerodynamic lens) via a small 2 mm orifice in the ring electrode, similar to Yang et al.'s [17] first design. The control software provides TTL triggers to fire the desorption laser and open the electron gate upon arrival of the particle in the center of the ion trap mass analyzer. A pulsed TEA-CO_2 laser (MTL-3G, Edinburgh Instruments Ltd.) is used for desorption. The MTL-3G is a single mode, tunable laser (9.2–10.8 μm) with a maximum output of 50 mJ on the strongest lines (~5×10^7 W/cm^2). The CO_2 desorption laser enters at a 35.2° angle between the ring and end cap to intersect with the particle in the center of the trap. A 250 mm ZnSe lens focuses the output of the CO_2 laser to a ~1 mm diameter spot inside the ion trap for particle desorption. The main pulse of the CO_2 laser is 140 ns wide followed by a ~1 μs broad tail.

All studies were performed at a desorption wavelength of 944 cm^{-1} due to its common use in previous two laser desorption ionization experiments [10,32,33]. The CO_2 energy used depended on the particle composition and size; in all cases, the highest energy possible that did not produce noticeable ions from the desorption step alone was chosen.

One factor affecting the uniformity of heating of a particle is the optical thickness of the material. A particle is optically thin if the product of the particle's radius, r, the absorption cross-section, σ, and the concentration, C, is $\ll$1, and thus the particle will be evenly heated [34]. The IR absorption cross-sections of 2,4-dihydroxybenzoic acid, caffeine, and oleic acid (the three molecules investigated in this study) were measured using a Bruker Equinox 55 FTIR and determined to be 2.38×10^{-20}, 9.00×10^{-21}, and 1.09×10^{-19} cm^2/molec, respectively at 944 cm^{-1}. Based on these numbers $r\sigma C \ll 1$ for our experimental conditions, and hence the particles should be uniformly heated. Additionally, as the wavelength of the CO_2 laser is much larger than the particle radius, there are no self-focusing issues within the particle that can lead to uneven heating [23]. These arguments suggest the particles should undergo an isotropic expansion after interaction with the CO_2 laser.

Following desorption, the gas-phase species are ionized with a 70 eV electron impact pulse, which is generated by an electron gun located behind the end cap opposite the ion detector. The electron gun consists of a rhenium hairpin filament/cathode held at 0 V and a cathode shield held at −70 V. The ion trap end cap is held at 0 V

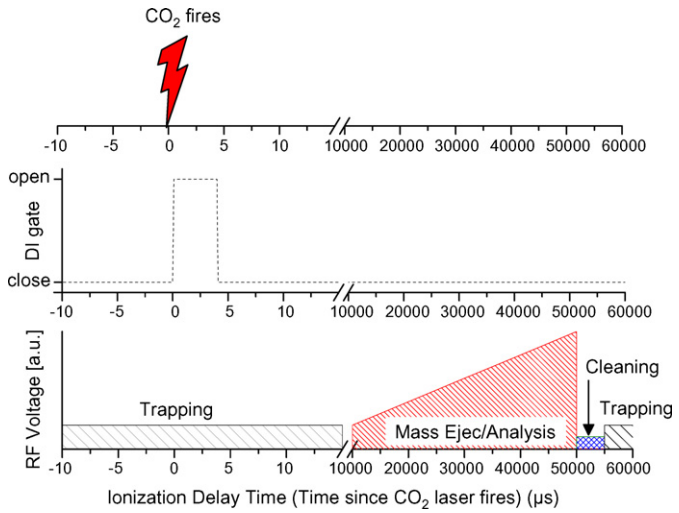

Fig. 2. Timing schematic for CO_2 laser firing, electron pulse from the electron gun and the RF voltage scan for the ion trap. Ionization delay times are referenced to the CO_2 firing. At 0 μs delay, the electron gun gate opens as the CO_2 laser is simultaneously discharging.

with a 1 mm entrance hole, which serves to accelerate the electrons when the filament/cathode is pulsed to −70 V. The home built electron gun used was designed to deliver about 50–100 μA total beam current. Based on comparative studies of gas-phase species using EI and VUV laser radiation [53], we estimate that the effective electron beam current inside the trap is on the order of 4 μA.

The timing scheme for desorption and ionization is detailed in Fig. 2. The delay time between the CO_2 laser firing and the EI gate opening is controlled by the data control/acquisition software and is referred to as "ionization delay time" subsequently in this work. Data can be collected at a fixed ionization delay time or the ionization delay time can be scanned. The opening of the electron gate is adjusted to generate a "pulsed" electron beam to optimally ionize single aerosols as they arrive in the trap. The width of the electron gate (or pulse of electrons) can be varied; unless otherwise noted a ~4 μs width was used for all experiments.

2.3.2. Mass analysis

Ions created in the EI process are trapped by applying a trapping potential from a customized QMS power supply (Extrel Mod 011-10; 0–5 kV V_P–V_P, 968 kHz RF frequency) to the ring electrode. The trap is periodically emptied by dropping the trapping potential to zero to avoid accumulation of background ions, coinciding with the laser charge times. Once the CO_2 laser and EI have fired, trapped ions are collisionally cooled for 10 ms in ~1 mTorr of He buffer gas and a mass scan is performed by linearly increasing the RF voltage (mass selective instability mode) [60].

Ions exit the trap through small holes in the end cap and are detected by an electron multiplier (ETP AF 138). Ion signals are amplified by a shaping amplifier (Keithley 427) and recorded by a 16-bit ADC Card (PCI-MIO-16XE-10, National Instruments) that is also used to create the RF ramp. After finishing the mass scan the trap is emptied and reset to the trapping voltage until the next aerosol event (or cleaning cycle). Supplemental AC waveforms can be applied to the end caps to either perform tandem mass spectrometry and/or conduct mass scans in resonant ejection mode, thereby extending the available mass range [61]. Waveforms are generated by an arbitrary waveform generator (PCI-5412, National Instruments) and amplified and inverted by a custom power supply.

In mass selective instability mode with this instrument, a mass range of 10–340 Th is accessible. This can be extended to about 2000 Th in resonant ejection mode, but this capability was not used in this study. Mass scanning rates of 4000 Th/s were used for all the experiments shown here, which led to analysis times of about 48 ms per mass spectrum. Under these conditions, about 5–10 particles/s can be analyzed, depending on the aerosol concentration in the sample flow. Mass resolution at 264 Th was typically around 500 ($m/\Delta m$). The mass axis is calibrated daily by recording 70 eV EI spectra of perfluorotributylamine.

Tandem mass spectrometry is implemented by applying supplemental SWIFT waveforms [61–64] to the ion trap end caps with in-house Labview software. After ion formation, trapping and cooling, a selected mass is isolated by applying two rounds of notched broadband waveforms for 5 ms and 10 ms with respective widths of 10 Th and 0.5 Th. The isolated ions then undergo collisionally induced dissociation with He buffer gas for 20 ms. Fragments are then mass analyzed. This procedure can be repeated for subsequent fragments to produce further spectral information (MS^3).

2.4. Chemicals

NIST traceable PSL nanosphere standards (Thermofisher, 3000 Series) were used to calibrate the SPIT-MS sizing region. The standards were diluted in MilliPore water and aerosolized with a medical nebulizer. The output was passed through the differential mobility analyzer (DMA) of a TSI SMPS 3936 operating at constant voltage. The flow was then split into a water based condensation particle counter (CPC, TSI Mod W3782) and the SPIT-MS. In this manner, both mobility diameter and aerodynamic size could be recorded, as well as respective particle count measurements to determine the particle detection efficiency.

Laboratory-generated aerosols of 2,4-dihydroxybenzoic acid (Fluka, ≥98%), caffeine (Aldrich, ≥98.5%), oleic acid (Aldrich, ≥99%), and linoleic acid (Aldrich, ≥99%) were used to test the combined sizing and mass analysis capabilities of the instrument. Chemicals were used without further purification. Particles were produced by aerosolizing solutions with the TSI Vibrating Orifice Aerosol Generator (TSI Inc., Model 3450) or TSI Constant Output Atomizer (TSI Inc., Model 3076). Oleic and linoleic acid solutions were prepared in 2-propanol (Aldrich, 99.9%). 2,4-dihydroxybenzoic acid and caffeine were prepared in Millipore water (18MΩ). Aerosols were passed through a ^{85}Kr charge neutralizer (TSI Mod 3054) as well as a 24" nafion diffusion dryer (Permapure Inc) before entering the SPIT-MS. This was done to ensure particle dryness and avoid size changes in the aerosol lens [65].

3. Results and discussion

3.1. Particle sizing region characterization

3.1.1. Sizer calibration

PSL nanosphere standards were used to calibrate the sizing module and ascertain instrumental performance. Fig. 3 shows the particle velocities as a function of vacuum aerodynamic diameter for the two laser setup and the one laser setup described above. Note that the different laser setups also required different alignments of the aerosol lens. Despite the measurements being taken 10 months apart and with very different sizing detection geometries, the total deviation between both datasets is <1%. This is significantly less than the 2–3% standard deviation of the individual velocity distributions.

Experimental particle velocities were fitted with the two-parameter function used in Zelenyuk et al. [9]:

$$v = v_o \cdot d_{va}^{c} = v_o \cdot \left(\frac{d_m \cdot \rho}{\chi}\right)^{c}$$

where v is the particle velocity, d_{va} is the particle vacuum aerodynamic diameter, d_m is the geometric diameter, ρ is the particle

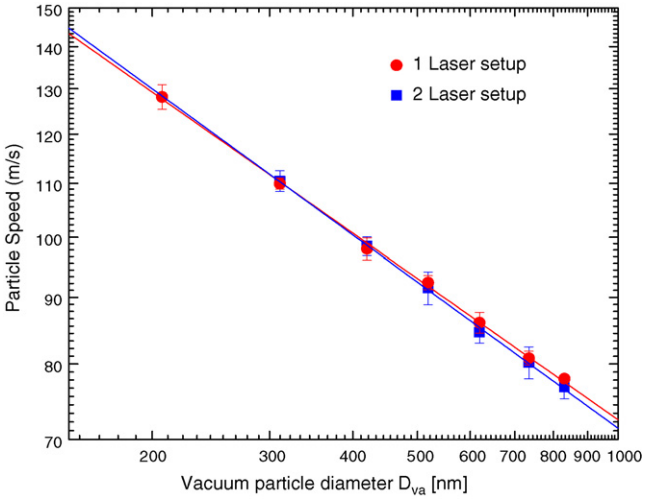

Fig. 3. Sizer calibration with PSLs for both the one and two laser setup.

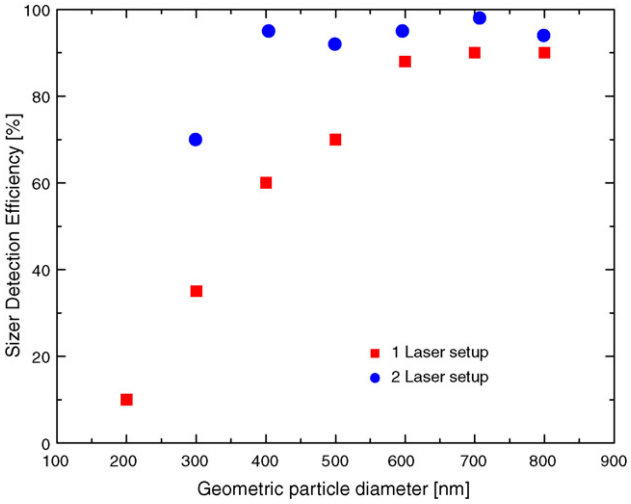

Fig. 4. Particle detection efficiencies (sized particles/sampled particles) for the PSL test aerosol measurements shown in Fig. 3. In the 1 laser case, small vertical adjustments in the sizing lasers were made to optimize detection at each size, while in the 2 laser case, one optical configuration was used for all measurements.

density, χ is the shape factor, and v_o and c are fit parameters. Fig. 3 shows the fits for PSL calibrations of the two alignment setups, where values for χ and and ρ_{part} of 1.01[66] and 1.05 g/mL (manufacturer specification), respectively were used. For the one laser setup the fit gave $v = 0.50785\, d_{va}^{(-0.3591)}$ and for the two laser setup, $v = 0.41775\, d_{va}^{(-0.37214)}$. In both cases r^2 is >99.9%. Based on the fit, the velocity distributions of unknown particle sizes can be converted into size distributions.

To illustrate the precision of the particle sizer, size distribution widths calculated from the measured PSL velocities are listed in Table 1.

Size distribution widths vary between ~2% at 400 nm and 4% at 700 nm, which is somewhat larger than the stated distributions widths of the manufacturer (Table 1). The higher precision for smaller particles is expected; although particle focusing and hence the precision of v actually slightly improve with increasing particle size, the power dependency of d_m results in decreasing sizing precision for larger, slower particles. For moderately spherical particles 4% seems to be a reasonably conservative estimate of the total sizing precision, while for liquid particles with smaller aerodynamic diameters precision is somewhat higher.

3.1.2. Sizing efficiencies

Sizing efficiencies were determined by comparing the number of aerosols sized by the instrument with the number of aerosols counted with the CPC running in parallel. The results for the two scattering laser arrangements (one laser setup and two laser setup) in the instrument are shown in Fig. 4. The results from the one laser setup were obtained by optimizing the vertical alignment of the laser with the particle beam at every size. The results from the two laser setup were obtained at the same alignment position for all sizes.

With our current lens, system pressures, and scattering detection arrangement, sizing efficiencies well over 90% are achievable for particles 400 nm and above. Zelenyuk et al. [35] reported sizing efficiencies close to 90% at 400 nm, which decreased towards larger sizes (10% at 800 nm). Harris et al. [20] reported 95% efficiency at 548 and 740 nm on their vertically mounted ion trap AMS, but did not provide data for other size ranges. Su et al. [56] in an ATOFMS upgrade for small particle sizes reported detection efficiencies around 42% for 300 nm particles.

The scattering detection limit of both Zelenyuk's instrument (SPLAT [35]) and Prather's instrument (ATOFMS [56]) for PSLs is significantly lower than the SPIT-MS's (~225 nm extrapolated for the current two laser configuration and alignment). As shown in Fig. 4, the detection limit actually decreased with the current scattering laser arrangement despite a higher laser intensity compared to the previous one laser setup. This is almost exclusively a function of the much larger amount of laser light scattered off the input windows in the new configuration, i.e., scattering response is currently background limited rather than signal limited. Installing an input baffle system similar to Zelenyuk et al.'s [9] should improve the detection limit substantially.

Vertical beam deflection of larger particle sizes can also be observed in the ion trap. In fact, optimum mass spectrometer hit rates for larger particles depend on a slight vertical adjustment of the desorption laser. It should be noted, however, that over a wide range of intermediate sizes (350–700 nm aerodynamic diameter) hardly any height adjustment of the desorption laser is necessary. The reproducibility of these measurements at all observation points and the fact that it was possible to observe this behavior in in-house CFD simulations of the aerosol lens leads us to believe that gravitational particle settling in the lens itself is responsible for this

Table 1
Width of the PSL calibration distributions recorded with the aerodynamic particle sizer (about 1000 particles per size) compared to the manufacturer's stated distributions widths.

PSL size [nm]	Sizing detection efficiency [%]	Manufacturer specified width σPSL [nm]	Measured size distribution width σTOF [nm]	Relative precision [%]
299	70	5.1	7.5	2.5
404	95	5.9	9.1	2.3
499	92	6.5	19.6	3.9
596	95	7.7	16.18	2.7
707	98	8.5	27.77	4
799	94	8.3	22.73	2.8

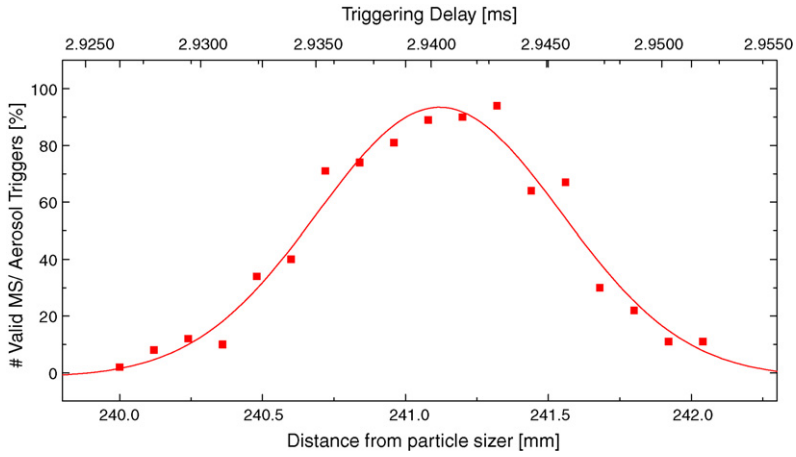

Fig. 5. Spatial profiles of MS hit rates (see text) for CO_2-only ionization of 970 nm DHB aerosols with 22 mJ/pulse ($\sim 3 \times 10^7$ W/cm^2) at 978 cm^{-1}. By varying the delay between the desorption laser and the aerosol trigger (top *X*-axis) the aerosols are exposed to different segments of the spatial CO_2 power profile, yielding a beam profile (bottom *X*-axis). The experimental data could be fitted to a simple Gaussian profile, as expected for a single mode TM_{00} laser.

behavior and that it is not related to machining imperfections in the lens [67].

The SPIT-MS performance with other particle types confirmed that regardless of density, phase or chemical composition, the scattering detection limit (detection limit for particle sizing region) for all test aerosols was between 210 and 240 nm geometric diameter, which is the region ($r_{part} \leq \lambda_{scatter}$) where scattering intensity for a 532 nm laser declines sharply. While particles with aerodynamic diameters up to 1500 nm can be detected with the SPIT-MS, it is currently not practical to sample particles in excess of ~1200 nm due to their large vertical displacement in the ion trap.

3.2. Characterization of the mass analysis region

To evaluate the overall transmission of particles into the ion trap and validate the performance of the triggering system, MS hit rates were recorded. MS hit rate is defined as the ratio of the number of identifiable aerosol mass spectra over the number of aerosol triggers provided by the particle sizer. In this work a given mass spectrum was classified as a valid aerosol spectrum if the integrated ion current at a particular mass was above a threshold level.

To validate the detection geometry and timing scheme, the CO_2 laser was operated at high energies to yield ions by simple laser ablation from 2,4-dihydroxybenzoic acid aerosols. Since ablation is expected to be less efficient than particle evaporation, this constitutes a lower limit for the LD-EI hit rate. By acquiring MS hit rates as a function of the delay between the last scattering event and the firing of the CO_2 laser, a convolution of the particle beam profile and the laser beam profile can be obtained as seen in Fig. 5. The fact that the maximum is over 90% confirms that both particle focusing and triggering work well.

The profile shown in Fig. 5 can also be used to corroborate the CO_2 laser beam geometry. Since the aerosol size (740 nm vacuum aerodynamic diameter) results in a small particle beam diameter (~100 μm), the profile should primarily reflect the shape of the laser beam. A Gaussian profile is observed, as expected for a single mode laser, and the measured width (1 mm after correcting for the 35.2° detection geometry) agrees very well with the diameter of laser beam burns taken at the center of the trap (0.9 ± 0.2 mm).

Given the proper CO_2 alignment and sufficiently high ion yields, overall detection efficiencies will stay constant over the whole range of accessible sizes.

3.3. Mass spectral identification of aerosols

Fig. 6 shows normalized single particle and 200 particle averaged mass spectra of 2,4-dihydroxybenzoic acid (879 nm geometric diameter) vaporized with 944 cm^{-1} (10.6 μm) IR pulses followed by 70 eV electron impact at the optimal ionization delay (in this case 1 μs). The 70 eV NIST spectrum of 2,4-dihydroxybenzoic acid is also shown for comparison [68]. The CO_2 energy used was 14 mJ/p (2×10^7 W/cm^2). No ion signal was observed from electron impact of undesorbed particles. The single particle mass spectrum provides an easily identifiable spectral fingerprint for 2,4-dihydroxybenzoic acid. The oscillation in the baseline in this experiment was due to RF pickup, which has been subsequently eliminated. The LD-EI parent and progeny ions match well with the expected fragmentation pattern, however, a higher percentage of smaller mass fragments are present in comparison to the literature spectrum.

Caffeine particles (887 nm diameter) were also investigated with LD-EI and demonstrated good correlation to the NIST spectrum [68] as shown in Fig. 7. A higher desorption energy (~30 mJ/p) was applied as the threshold for onset of ions from the CO_2 laser alone was greater in comparison to 2,4-dihydroxybenzoic acid (discussed

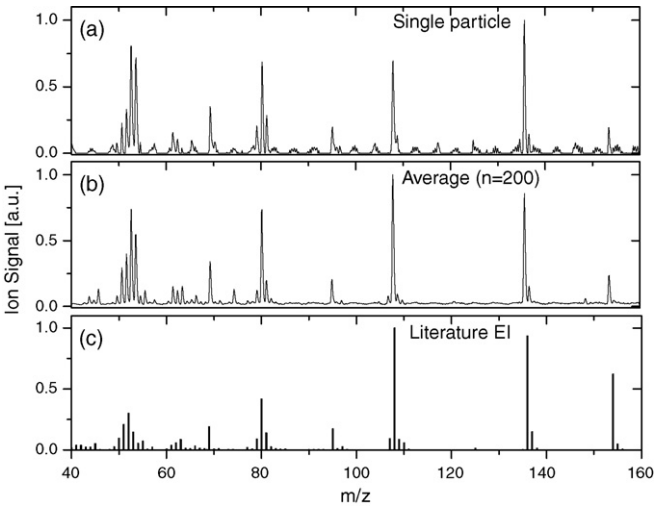

Fig. 6. Normalized spectra of (a) single particle and (b) 200 particle average of 2,4-dihydroxybenzoic acid (879 nm particles) collected with 14 mJ 944 cm^{-1} CO_2, 1 μs ionization delay and (c) NIST standard.

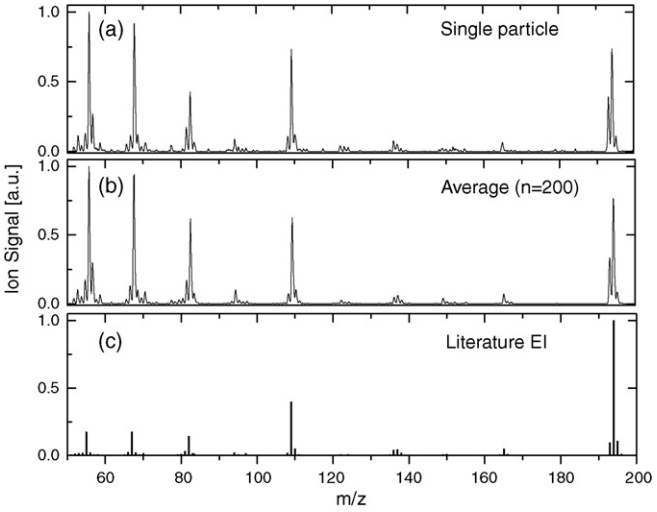

Fig. 7. Normalized spectra of (a) single particle and (b) 200 particle average of caffeine (887 nm particles) collected with 30 mJ 944 cm^{-1} CO_2, 1 μs ionization delay and (c) NIST standard.

later in the section on vaporization energy effects). Similar to the above observations for 2,4-dihydroxybenzoic acid, a higher percentage of lower *m*/*z* peaks are present in comparison to literature values.

Since the EI spectra of gas-phase chemicals measured with an ion trap agree with literature spectra provided that the storage time is not prolonged [69], the increased levels of fragmentation observed in both 2,4-dihydroxybenzoic acid and caffeine suggest that the energy imparted from the laser desorption step is higher than that from the thermal desorption used for NIST standards. Woods et al. [38] showed that with increasing CO_2 energy, the fragmentation pattern shifted towards a larger percentage of lower *m*/*z* ions. Other studies have also demonstrated the effects of imparting increased internal energy during desorption on fragmentation patterns via both cartridge heaters and CO_2 laser [70–73]. As NIST standards are typically collected at a temperature that produces signal (2,4-dihydroxybenzoic acid, 220 °C and caffeine, 250 °C) rather than necessarily achieving complete vaporization, it is not surprising that the laser desorption in our experiment imparts more energy to the molecules prior to EI, resulting in increased fragmentation.

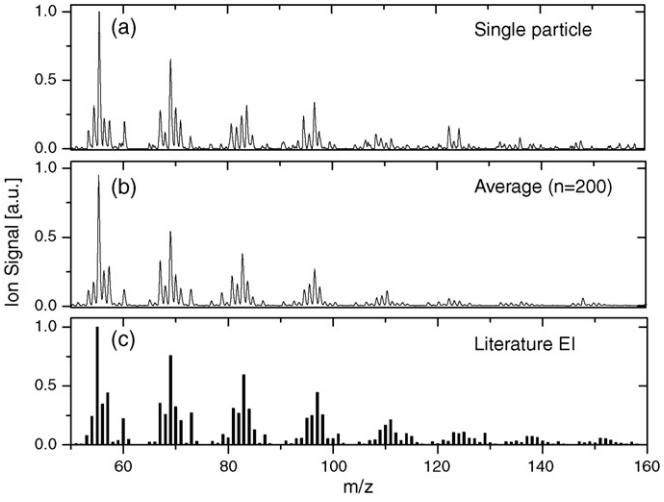

Fig. 8. Normalized spectra of (a) single particle and (b) 200 particle average of oleic acid (1.1 μm particles) collected with 15 mJ 944 cm^{-1} CO_2, 1 μs ionization delay and (c) NIST standard.

Additionally, oleic and linoleic acid, both liquid aerosols, were briefly investigated with LD-EI. Normalized single particle and 200 particle averaged spectra at 1 μs ionization delay and the EI NIST standard [68] are shown in Fig. 8 for oleic acid. Single particle and averaged spectra for linoleic acid were also collected and closely matched the EI NIST standard (not shown). The geometric particle diameter used for liquids (~1 μm) was larger than for solid particles as similar aerodynamic diameters were selected for comparison. Although oleic and linoleic acid differ only by 2 Th, the observed fragmentation ratios of the pure aerosols reflected unique mass spectral fingerprints that permit the two species to be distinguished. Parent ions were not observed for either oleic or linoleic acid, which is similar to results from other studies of aliphatics fragmented by electron impact [74].

3.4. MS^n performance

The MS^n capabilities of our single particle LD-EI mass spectrometer were demonstrated using caffeine particles. Fig. 9 shows a MS/MS study of caffeine particles (887 nm diameter) with an average of 200 particles displayed for each panel. In Fig. 9a, the standard mass spectrum of ions produced from 30 mJ CO_2 with EI is shown. This EI spectrum is comparable to Verenitch et al.'s work with GC–MS (EI ionization) of caffeine. 194 Th is the parent ion M^+, 193 Th is $[M-H]^+$, 165 Th is $[M-CO-H]^+$,137 Th is $[M-H-CH_3NCO]^+$, 109 Th is $[M-CH_3NCO-CO]^+$, and 82 Th is $[M-CH_3NCO-CO-HCN]^+$. The parent peak at 194 Th was subsequently isolated (Fig. 9b) with an average efficiency of 52%. Collisionally induced dissociation by resonant excitation of 194 Th produced predominantly 193 Th as shown in Fig. 9c, along with 165, 137 and 109 Th. Further isolation and CID of the MS^2 fragment at 193 Th produced a range of ions at 165, 149 $[M-H-CO_2]^+$, 134 $[M-H-CO_2-CH_3]^+$, 122 $[M-H-CO_2-HCN]^+$, 120 $[M-H-CO_2-H_2CN]^+$, and 108 Th (which can stem from 2 fragments) as seen in Fig. 9d. The overall efficiency for MS^3 is approximately 15%. It is worth noting that Verenitch et al.'s MS/MS spectrum for caffeine is an amalgamation of the spectra produced in Fig. 9c and d, indicating their process likely imparted more energy during CID of the parent ion than the waveform used in this study [75].

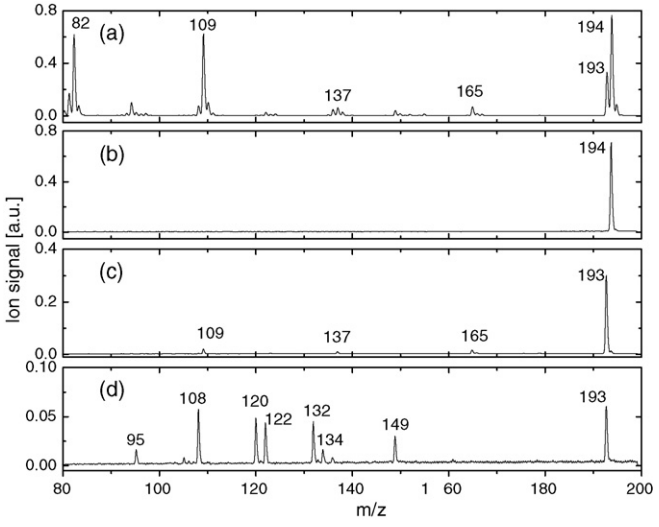

Fig. 9. A sequence of MS/MS studies performed for ions from caffeine aerosols, desorbed with 30 mJ CO_2 and recorded with 1 μs ionization delay. (a) Caffeine aerosol MS, (b) isolation of parent peak (194 Th), (c) fragmentation of parent peak via collisionally induced dissociation, (d) subsequent fragmentation of 193 Th.

3.5. Effect of operational parameters on mass spectra

3.5.1. Dependence of total ion signal on laser desorption energy

Mass spectra of pure 2,4-dihydroxybenzoic acid (1 μm diameter) and caffeine (887 nm diameter) particles were collected at varying CO_2 laser powers. The respective energy ranges used for each species were selected by determining the energy required for ion generation via CO_2 laser alone and then limiting measurements to energies below that level. Fig. 10 shows the total ion signal (summation of parent and main progeny peaks) for each species integrated over a portion of the ionization delay time scan where S/N is above the detection limit. Each point represents an average of 300 shots. Total ion signal for 2,4-dihydroxybenzoic acid plateaus at 10–12 mJ/p, while the signal for caffeine is not observed to plateau within the range of energies studied. (It should be noted that a previous study of an 879 nm DHB particle reached a plateau in total ion signal in the same range as the 1 μm particle.) The IR absorption cross-sections (see Section 2.3.1) measured at 944 cm^{-1} for the two species (DHB = 2.38×10^{-20} cm^2/molec and caffeine = 9.00×10^{-21} cm^2/molec) are consistent with DHB reaching a plateau at lower CO_2 energies than caffeine. The DHB plateau of total signal with laser vaporization energy suggests that beyond a certain desorption energy or threshold, the total signal remains constant regardless of CO_2 energy and may indicate near complete or complete vaporization [10,76].

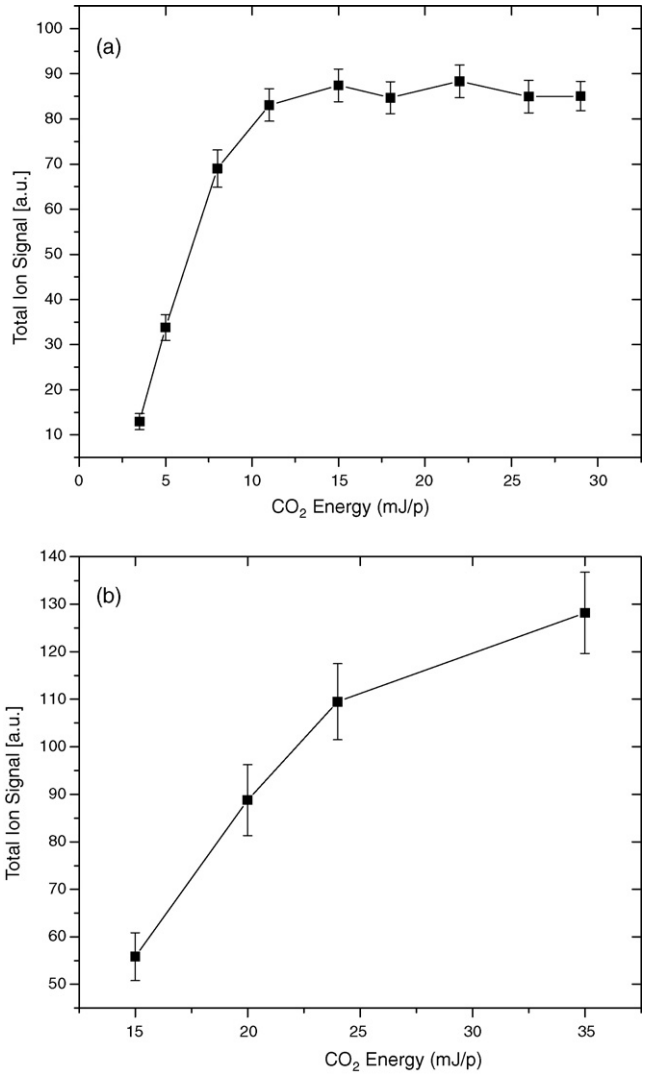

Fig. 10. Total ion signal as a function of CO_2 energy (944 cm^{-1}) for (a) 2,4-dihydroxybenzoic acid [154, 136, 108, 95, 80, 69, 64, 53 Th] and (b) caffeine [194, 193, 109, 82, 81, 67, 55 Th].

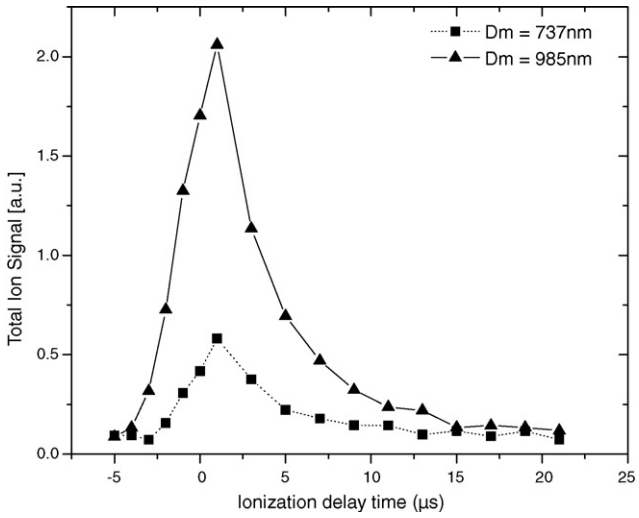

Fig. 11. Total ion signal [154, 136, 108, 80, 69 Th] versus the ionization delay time (time between the desorption laser firing and the electron pulse) at 14 mJ 944 cm^{-1} for 2,4-dihydroxybenzoic acid of two different particle sizes (D_m shown).

3.5.2. Dependence of total ion signal on ionization delay time (time between firing the CO_2 laser and the electron pulse)

The results from scanning the ionization delay time are illustrated in Fig. 11 for two sizes of 2,4-dihydroxybenzoic acid particles. In this mode the onset of ion signal is observed as the electron pulse (~4 μs long) overlaps the firing of the CO_2 laser, rising to a maximum signal at the optimal ionization delay (time between the desorption/ionization steps) and then subsequent decay as the gas-phase expands outside of the trapping volume. A signal at a negative ionization delay time merely reflects the ionization delay being defined relative to the CO_2 laser firing. The maximum signal generally occurs at a 0 or 1 μs delay, after a 3–5 μs rise (time from no signal) with slight variability based on desorption energy. This is the expected behavior for our system based on the electron gate width and the expansion of the neutral plume in the trap. The delay profile observed is roughly comparable to that obtained in Cabalo et al.'s system [77].

3.5.3. Dependence of total ion signal on electron gate pulse width

Fig. 12 illustrates the ion signal at 136 Th as a function of ionization delay time for a 2,4-dihydroxybenzoic acid particle studied with three different gate widths, all using 14 mJ CO_2 for vaporization. Increasing the gate width enhances the ion signal to a maximal point after which no further effect on ion signal is achieved. Conversely, increasing the gate width reduces the time resolution of delay scans such that the temporal characteristics of the profile expansion are obscured. Although the gate width could be expanded to 10–13 μs to increase signal and enhance our detection limit for routine measurements, the 4 μs gate width was used in these experiments to (a) allow us to investigate the profile of the neutral expansion post-desorption and (b) minimize any signal from background residual gases.

Also shown in Fig. 12 is the ionization delay time scan from a CO_2-VUV study of 2,4-dihydroxybenzoic acid in the SPIT-MS setup described by Hanna et al. [53]. In this case, the ionization delay time refers to the time between the CO_2 laser firing (15 mJ 944 cm^{-1} desorption) and the VUV laser firing (144 nm). The VUV laser pulse is 5 ns long which provides excellent time resolution. As can be seen, the full-width half maximum of the VUV profile is only ~1 μs

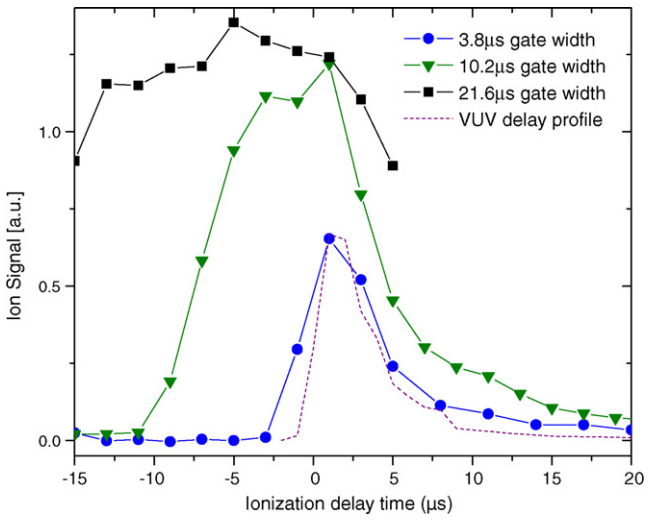

Fig. 12. Effect of EI gate width on ion signal as a function of ionization delay time and comparison with a high resolution time scan using pulsed VUV light for ionization [53]. The VUV profile has been adjusted in time so that the maximum signal overlaps with the EI 4 μs gate width profile.

shorter than that for the 4 μs EI gate width. This implies that at standard settings the resolution of the LD-EI experiment is nearly comparable. In fact, a 4 μs running average of the scaled VUV profile exactly matches the EI profile, further supporting this conclusion.

3.5.4. Dependence of fragment abundances on ionization delay time

Fig. 13 illustrates the ratio of individual peak signal to total ion signal for caffeine (887 nm diameter particle) as a function of ionization delay time. Each data point is an average of 300 shots. At delay times between −5 and −2 μs, the relative error is significant and *S*/*N* values are meaningless due to the low number of valid particle spectra collected, if any are observed at all. For this reason, a restricted range is selected for the integrated delay scan analysis where the *S*/*N* ratio is above the detection limit and relative error is low.

Similar to previous works [38,72], we observe that the degree of fragmentation depends on the ionization delay time (Fig. 13).

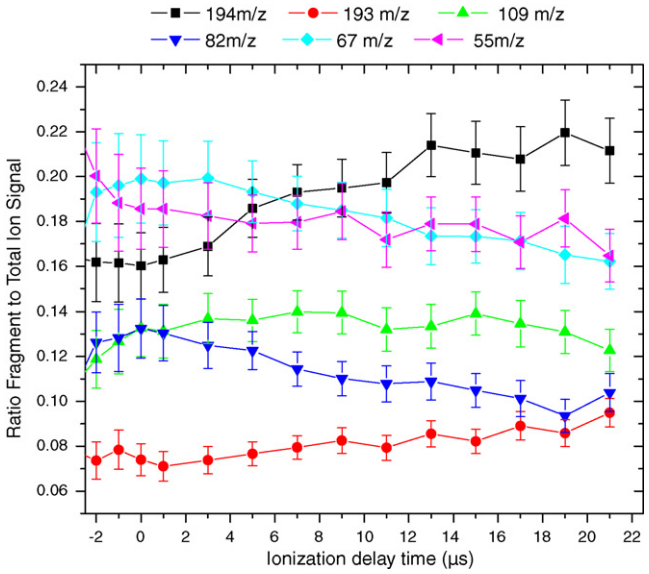

Fig. 13. Ratio of parent or progeny to total ion signal for caffeine as a function of ionization delay time at 35 mJ 944 cm^{-1} CO_2.

After −2 μs delay, the percent of the parent 194 Th ion increased with ionization delay time while the 82, 67, and 55 Th progeny peaks decreased in intensity. A parallel effect was observed for 2,4-dihydroxybenzoic acid (879 nm particle). As Fig. 13 shows, at longer ionization delays fragmentation could be minimized, however the significance of such an effect may depend on the particle composition and morphology and comes at the expense of the total signal being reduced. The change in percent abundance of parent ion is less significant at low vaporization energies for both species studied. Some explanations for the dependence of fragmentation on delay time have been previously discussed by others in significant detail and will not be included here [38,78].

3.6. Detection limit

We have acquired LD-EI spectra from a range of DHB particle sizes down to 325 nm diameter, where MS signal is still distinguishable from background signal (*S*/*N* is ∼2). Given the *S*/*N* ratio, we appear to be virtually at our detection limit for this molecule. This size corresponds to a detection limit of 8.7×10^7 molecules. This number is consistent with the gas-phase detection limit we determined for our EI-ion trap in separate experiments using toluene as a calibration gas (8×10^7 molecules).

The electron gun (see Fig. 12) used for these experiments was designed solely for the purpose of ionizing calibration gas when originally constructed and is by no means optimized for beam current or shape, nor has the electron beam been thoroughly characterized. Additionally, since the electron gun is recessed behind one of the end caps, the RF field undoubtedly distorts the electron beam. The ultimate detection limit of this technique could potentially be improved by a superior filament shape (minimizing the emitting area), changing the filament height, better alignment through the trap, increasing the duration of the electron pulse (increasing electron flux by a factor of 2) or enhancing the brilliance of the electron pulse. Varying the anode voltage as well as minimizing the electron beam focus [79] may optimize the peak current obtained. Adjusting the energy level to less than 70 eV to reduce fragmentation is also a possibility, but at the cost of signal that would, in turn, limit the detection of single particles.

Acknowledgements

This work was performed at the UBC Laboratory for Advanced Spectroscopy and Imaging Research (LASIR). The authors would like to thank the National Sciences and Engineering Research Council of Canada (NSERC), the Canadian Foundation for Climate and Atmospheric Sciences (CFCAS), the Canadian Foundation for Innovation (CFI), the British Columbia Knowledge Development Fund (BCKDF), the NRC-NSERC-BDC Nanotechnology Initiative, and the Canada Research Chair Program for financial support.

References

[1] U. Pöschel, Angew. Chem. Int. Ed. 44 (2005) 7520.
[2] M. Kanakidou, J.H. Seinfeld, S.N. Pandis, I. Barnes, F.J. Dentener, M.C. Facchini, R. Van Dingenen, B. Ervens, A. Nenes, C.J. Nielsen, E. Swietlicki, J.P. Putaud, Y. Balkanski, S. Fuzzi, J. Horth, G.K. Moortgat, R. Winterhalter, C.E.L. Myhre, K. Tsigaridis, E. Vignati, E.G. Stephanou, J. Wilson, Atmos. Chem. Phys. 5 (2005) 1053.
[3] S. Fuzzi, M.O. Andreae, B.J. Huebert, M. Kulmala, T.C. Bond, M. Boy, S.J. Doherty, A. Guenther, M. Kanakidou, K. Kawamura, V.M. Kerminen, U. Lohmann, L.M. Russell, U. Poschl, Atmos. Chem. Phys 6 (2006) 2017.
[4] P.F. DeCarlo, J.R. Kimmel, A. Trimborn, M.J. Northway, J.T. Jayne, A.C. Aiken, M. Gonin, K. Fuhrer, T. Horvath, K.S. Docherty, D.R. Worsnop, J.L. Jimenez, Anal. Chem. 78 (2006) 8281.
[5] E. Gard, J.E. Mayer, B.D. Morrical, T. Dienes, D.P. Fergenson, K.A. Prather, Anal. Chem. 69 (1997) 4083.
[6] H.J. Tobias, P.M. Kooiman, K.S. Docherty, P.J. Ziemann, Aerosol Sci. Technol. 33 (2000) 170.

[7] J.T. Jayne, D.C. Leard, X.F. Zhang, P. Davidovits, K.A. Smith, C.E. Kolb, D.R. Worsnop, Aerosol Sci. Technol. 33 (2000) 49.
[8] F. Drewnick, S.S. Hings, P. DeCarlo, J.T. Jayne, M. Gonin, K. Fuhrer, S. Weimer, J.L. Jimenez, K.L. Demerjian, S. Borrmann, D.R. Worsnop, Aerosol Sci. Technol. 39 (2005) 637.
[9] A. Zelenyuk, D. Imre, Aerosol Sci. Technol. 39 (2005) 554.
[10] E. Woods, G.D. Smith, Y. Dessiaterik, T. Baer, R.E. Miller, Anal. Chem. 73 (2001) 2317.
[11] B.W. LaFranchi, J. Zahardis, G.A. Petrucci, Rapid Commun. Mass Spectrom. 18 (2004) 2517.
[12] R. Mahadevan, D. Lee, H. Sakurai, M.R. Zachariah, J. Phys. Chem. A 106 (2002) 11083.
[13] P.J. Mckeown, M.V. Johnston, D.M. Murphy, Anal. Chem. 63 (1991) 2069.
[14] A. Zelenyuk, J. Cabalo, T. Baer, R.E. Miller, Anal. Chem. 71 (1999) 1802.
[15] J.M. Dale, M. Yang, W.B. Whitten, J.M. Ramsey, Anal. Chem. 66 (1994) 3431.
[16] M. Yang, J.M. Dale, W.B. Whitten, J.M. Ramsey, Anal. Chem. 67 (1995) 1021.
[17] M. Yang, P.T.A. Reilly, K.B. Boraas, W.B. Whitten, J.M. Ramsey, Rapid Commun. Mass Spectrom. 10 (1996) 347.
[18] P.T.A. Reilly, R.A. Gieray, M. Yang, W.B. Whitten, J.M. Ramsey, Anal. Chem. 69 (1997) 36.
[19] A. Lazar, P.T.A. Reilly, W.B. Whitten, J.M. Ramsey, Environ. Sci. Technol. 33 (1999) 3993.
[20] W.A. Harris, P.T.A. Reilly, W.B. Whitten, J.M. Ramsey, Rev. Sci. Instrum. 76 (2005).
[21] A. Kürten, J. Curtius, F. Helleis, E.R. Lovejoy, S. Borrmann, Int. J. Mass Spectrom. 265 (2007) 30.
[22] A.C. Lazar, P.T.A. Reilly, W.B. Whitten, J.M. Ramsey, Anal. Chem. 72 (2000) 2142.
[23] W.A. Harris, P.T.A. Reilly, W.B. Whitten, Int. J. Mass Spectrom. 258 (2006) 113.
[24] B.A. Mansoori, M.V. Johnston, A.S. Wexler, Anal. Chem. 66 (1994) 3681.
[25] M.V. Johnston, J. Mass Spectrom. 35 (2000) 585.
[26] H. Coe, J.D. Allan, Mass spectrometric methods for aerosol composition measurements, in: D.E. Heard (Ed.), Analytical Techniques for Atmospheric Measurement, Blackwell Publishing, Oxford, 2006.
[27] W.A. Harris, P.T.A. Reilly, W.B. Whitten, Anal. Chem. 79 (2007) 2354.
[28] T. Hoffmann, R. Bandur, U. Marggraf, M. Linscheid, J. Geophys. Res. [Atmos.] 103 (1998) 25569.
[29] C.N. Dalton, M. Jaoui, R.M. Kamens, G.L. Glish, Anal. Chem. 77 (2005) 3156.
[30] S.T. Quarmby, R.A. Yost, Int. J. Mass Spectrom. 191 (1999) 81.
[31] P.T.A. Reilly, A.C. Lazar, R.A. Gieray, W.B. Whitten, J.M. Ramsey, Aerosol Sci. Technol. 33 (2000) 135.
[32] B.D. Morrical, D.P. Fergenson, K.A. Prather, J. Am. Soc. Mass Spectrom. 9 (1998) 1068.
[33] M. Bente, T. Adam, T. Ferge, S. Gallavardin, M. Sklorz, T. Streibel, R. Zimmermann, Int. J. Mass Spectrom. 258 (2006) 86.
[34] T. Ferge, F. Mühlberger, R. Zimmermann, Anal. Chem. 77 (2005) 4528.
[35] A. Zelenyuk, Y. Cai, L. Chieffo, D. Imre, Aerosol Sci. Technol. 39 (2005) 972.
[36] C. Focsa, C. Mihesan, M. Ziskind, B. Chazallon, E. Therssen, P. Desgroux, J.L. Destombes, J. Phys.: Condens. Matter 18 (2006) S1357.
[37] E. Woods, G.D. Smith, R.E. Miller, T. Baer, Anal. Chem. 74 (2002) 1642.
[38] E. Woods, R.E. Miller, T. Baer, J. Phys. Chem. A 107 (2003) 2119.
[39] E. Parra, I. Alexeev, J.Y. Fan, K.Y. Kim, S.J. McNaught, H.M. Milchberg, J. Opt. Soc. Am. B: Opt. Phys. 20 (2003) 118.
[40] C. Menzel, K. Dreisewerd, S. Berkenkamp, F. Hillenkamp, J. Am. Soc. Mass Spectrom. 13 (2002) 975.
[41] D.M. Murphy, Mass Spectrom. Rev. 26 (2007) 150.
[42] J.L. Jimenez, J.T. Jayne, Q. Shi, C.E. Kolb, D.R. Worsnop, I. Yourshaw, J.H. Seinfeld, R.C. Flagan, X.F. Zhang, K.A. Smith, J.W. Morris, P. Davidovits, J. Geophys. Res. [Atmos.] 108 (2003).
[43] S.T. Fountain, D.M. Lubman, Anal. Chem. 65 (1993) 1257.
[44] Z.M. Yuan, C. Fenselau, D.M. Dulik, W. Martin, W.B. Emary, R.B. Brundrett, O.M. Colvin, R.J. Cotter, Anal. Chem. 62 (1990) 868.
[45] F. Drewnick, P.H. Wieser, Rev. Sci. Instrum. 73 (2002) 3003.
[46] K.A. Lincoln, Int. J. Mass Spectrom. Ion Phys. 2 (1969) 75.
[47] K.A. Lincoln, Int. J. Mass Spectrom. Ion Phys. 13 (1974) 45.
[48] R.B. Vanbreemen, M. Snow, R.J. Cotter, Int. J. Mass Spectrom. Ion Processes 49 (1983) 35.
[49] C. Fenselau, W.B. Emary, R.J. Cotter, Org. Mass Spectrom. 24 (1989) 694.
[50] D.G. Nash, T. Baer, M.V. Johnston, Int. J. Mass Spectrom. 258 (2006) 2.
[51] C.A. Noble, K.A. Prather, Mass Spectrom. Rev. 19 (2000) 248.
[52] A.S. Wexler, M.V. Johnston, Real-time single-particle analysis, in: P.A. Baron, K. Willeke (Eds.), Aerosol Measurements: Principles, Techniques, and Applications, John Wiley, New York, 2001.
[53] S.J. Hanna, P. Campuzano-Jost, E.A. Simpson, D.B. Robb, M.W. Blades, J.W. Hepburn, A.K. Bertram, Int. J. Mass Spectrom. 279 (2009) 134.
[54] P. Liu, P.J. Ziemann, D.B. Kittelson, P.H. Mcmurry, Aerosol Sci. Technol. 22 (1995) 293.
[55] P. Liu, P.J. Ziemann, D.B. Kittelson, P.H. Mcmurry, Aerosol Sci. Technol. 22 (1995) 314.
[56] Y.X. Su, M.F. Sipin, H. Furutani, K.A. Prather, Anal. Chem. 76 (2004) 712.
[57] P.S.K. Liu, R. Deng, K.A. Smith, L.R. Williams, J.T. Jayne, M.R. Canagaratna, K. Moore, T.B. Onasch, D.R. Worsnop, T. Deshler, Aerosol Sci. Technol. 41 (2007) 721.
[58] X.F. Zhang, K.A. Smith, D.R. Worsnop, J.L. Jimenez, J.T. Jayne, C.E. Kolb, J. Morris, P. Davidovits, Aerosol Sci. Technol. 38 (2004) 619.
[59] X.F. Zhang, K.A. Smith, D.R. Worsnop, J. Jimenez, J.T. Jayne, C.E. Kolb, Aerosol Sci. Technol. 36 (2002) 617.
[60] R.E. March, Rapid Commun. Mass Spectrom. 12 (1998) 1543.
[61] V.M. Doroshenko, R.J. Cotter, Rapid Commun. Mass Spectrom. 10 (1996) 65.
[62] M.H. Soni, R.G. Cooks, Anal. Chem. 66 (1994) 2488.
[63] R.K. Julian, R.G. Cooks, Anal. Chem. 65 (1993) 1827.
[64] D.E. Goeringer, S.A. McLuckey, J. Chem. Phys. 104 (1996) 2214.
[65] A. Zelenyuk, D. Imre, L.A. Cuadra-Rodriguez, Anal. Chem. 78 (2006) 6942.
[66] Y. Katrib, S.T. Martin, Y. Rudich, P. Davidovits, J.T. Jayne, D.R. Worsnop, Atmos. Chem. Phys. 5 (2005) 275.
[67] J.A. Huffman, J.T. Jayne, F. Drewnick, A.C. Aiken, T. Onasch, D.R. Worsnop, J.L. Jimenez, Aerosol Sci. Technol. 39 (2005) 1143.
[68] S.E. Stein, Mass Spectra, in: P.J. Linstrom, W.G. Mallard (Eds.), NIST Chemistry WebBook, NIST Standard Reference Database Number 69, National Institute of Standards and Technology, Gaithersburg, MD, 2005.
[69] R.E. March, Tandem Mass Spectrometry, in: R.E. March, J.F.J. Todd (Eds.), Practical Aspects of Ion Trap Mass Spectrometry: Chemical, Environmental, and Biomedical Applications, CRC Press, Inc., Boca Raton, 1995, p. 34.
[70] M.J. Northway, J.T. Jayne, D.W. Toohey, M.R. Canagaratna, A. Trimborn, K.I. Akiyama, A. Shimono, J.L. Jimenez, P.F. DeCarlo, K.R. Wilson, D.R. Worsnop, Aerosol Sci. Technol. 41 (2007) 828.
[71] K.R. Wilson, M. Jimenez-Cruz, C. Nicolas, L. Belau, S.R. Leonet, M. Ahmed, J. Phys. Chem. A 110 (2006) 2106.
[72] D.G. Nash, X.F. Liu, E.R. Mysak, T. Baer, Int. J. Mass Spectrom. 241 (2005) 89.
[73] E.R. Mysak, K.R. Wilson, M. Jimenez-Cruz, M. Ahmed, T. Baer, Anal. Chem. 77 (2005) 5953.
[74] M.R. Canagaratna, J.T. Jayne, J.L. Jimenez, J.D. Allan, M.R. Alfarra, Q. Zhang, T.B. Onasch, F. Drewnick, H. Coe, A. Middlebrook, A. Delia, L.R. Williams, A.M. Trimborn, M.J. Northway, P.F. DeCarlo, C.E. Kolb, P. Davidovits, D.R. Worsnop, Mass Spectrom. Rev. 26 (2007) 185.
[75] S.S. Verenitch, A. Mazumder, Anal. Bioanal. Chem. 391 (2008) 2635.
[76] D.C. Sykes, E. Woods, G.D. Smith, T. Baer, R.E. Miller, Anal. Chem. 74 (2002) 2048.
[77] J. Cabalo, A. Zelenyuk, T. Baer, R.E. Miller, Aerosol Sci. Technol. 33 (2000) 3.
[78] E. Woods, Y. Dessiaterik, R.E. Miller, T. Baer, J. Phys. Chem. A 105 (2001) 8273.
[79] M.S. Ragheb, S.G. Zakhary, Radiat. Phys. Chem. 58 (2000) 1.